IEEE Access
Multidisciplinary | Rapid Review | Open Access Journal

Date of publication xxxx 00, 0000, date of current version xxxx 00, 0000.

Digital Object Identifier 10.1109/ACCESS.2021.DOI

Channel Estimation via Model and Learning for Monostatic Multiantenna Backscatter Communication

MOLDIR YERZHANOVA[1] and YUN HEE KIM[12], *Senior Member, IEEE*
[1]Department of Electronics and Information Convergence Engineering, Kyung Hee University, Yongin 17104, Korea (e-mail: moldir.yerzhanova@khu.ac.kr, yheekim@khu.ac.kr)
[2]Department of Electronic Engineering, Kyung Hee University, Yongin 17104, Korea.

Corresponding author: Yun Hee Kim (e-mail: yheekim@khu.ac.kr).

This work was supported by Ministry of Science and ICT, Korea, through the National Research Foundation of Korea (NRF) under the Grant NRF-2021R1A2C1005869 and the Institute for Information & Communications Technology Planning & Evaluation (IITP) under the Information Technology Research Center support program (IITP-2021-0-02046).

ABSTRACT Backscatter communication has received considerable attention for future Internet-of-things (IoT) designed with battery-free devices. To support massive connectivity of such energy-constrained IoT devices, a monostatic multiantenna backscatter communication network (MBCN) with beamforming has emerged, for which reliable channel estimation is indispensable. This paper tackles backscatter and forward channel estimation problems for a monostatic MBCN in a generalized fading model, where the optimal minimum mean square error (MMSE) solutions are too intricate to derive due to the cascaded backscatter channel. After deriving the linear MMSE (LMMSE) estimator of the backscatter channel in the generalized fading model, we propose learning-based estimators based on the fast and flexible convolutional neural network (FFDNet) toward the optimal solution. We also propose a deep neural network (DNN) with a customized loss function that estimates the forward channel coefficients directly from the backscattered signal. The results show that the proposed FFDNet-based estimator for the backscatter channel reduces the MSE of the LMMSE estimator by a factor of two and three. In addition, the DNN-based estimator for the forward channel is shown to reduce the pilot overhead up to by half when compared with the conventional estimator.

INDEX TERMS Backscatter communication, channel estimation, deep learning, linear minimum mean square error, multiple antennas

I. INTRODUCTION

BACKSCATTER communication has been reemerged as one of key enabling technologies for sustainable Internet-of-things (IoT) supporting massive energy-constrained devices proliferating everywhere [1]–[4]. A backscatter device (BD) modulates its data by reflecting an incident carrier from another source instead of generating its own carrier, which alleviates a large portion of power consumption at active radio frequency (RF) circuits in generating a carrier [1]. In this way, BDs are kept sustainable for a long period without battery replacement or even without a battery. Backscatter communication is now evolving from low rate applications like RF identification to high-performance IoT applications by addressing coding, high order modulation, and multiple access schemes [5]–[7].

Backscatter communication networks (BCNs) have emerged in various forms according to a source generating a carrier and a reader demodulating a backscattered signal. Monostatic BCNs embed a source and a reader in the same entity [8]–[17] whilst bistatic and ambient BCNs embed them in different entities [18]–[22]; A bistatic BCN deploys its own source dedicated to that BCN [18], [22] but an ambient BCN utilizes a nearby transmitter deployed for another service as its carrier source [19]–[21]. Each BCN type has its own pros and cons so that it has been developed in a way of making good use of its advantages.

The monostatic BCN, of our concern, is prone to a centralized communication with multiple devices similar to a cellular network [8], [10], [13]–[17]. Thus, a hybrid access point (HAP) of a monostatic BCN sending a carrier as well as receiving its backscatterd signal has evolved to support multiple BDs through various multiple access schemes. In particular, multiple antennas at the HAP were shown to elevate the energy and rate transfer by optimizing transmit

This article has been accepted for publication in a future issue of this journal, but has not been fully edited. Content may change prior to final publication. Citation information: DOI 10.1109/ACCESS.2021.3134961, IEEE Access

beamforming for carrier transmission and receive beamforming for backscatter demodulation [8], [13], [14], [17].

For receive beamforming and coherent demodulation, the HAP needs to estimate the backscatter channel that is formed by multiplying the forward channel from the HAP to a BD and the reverse channel from the BD to the HAP. To implement transmit beamforming, the HAP requires the channel state information (CSI) on the forward channel. In a BCN, it is desirable for channel estimation to be performed at the HAP rather than at an energy constrained BD that would suffer from inevitable power consumption for channel estimation and CSI feedback. Channel estimation at the HAP can be accomplished by transmitting a pilot-embedded carrier to a BD and estimating the channels from the backscattered pilot signal [8], [12], [14], [15]. For a full-duplex monostatic BCN with channel reciprocity, model-based channel estimators were studied for the backscatter and forward channels with full and reduced pilot overhead [12], [14], [15]; the least square (LS) and linear minimum mean square error (LMMSE) criteria were adopted for backscatter multiple input multiple output (MIMO) channel estimation and eigen-decomposition (EVD) of a backscatter channel estimate followed by decorrelation was proposed for forward channel estimation. However, the studies were limited to the simplest forward channel model of uncorrelated Rayleigh fading.

Recently, learning-based channel estimators have been studied to provide solutions competitive to model-based ones without resorting to tedious mathematical computation and prior statistical information [23]–[30]. On the one hand, deep neural networks (DNNs) have been applied to estimate the channel coefficients of MIMO systems [23]–[25]. On the other hand, deep denoising networks based on convolutional neural networks (CNNs) have been applied for channel estimation in various wireless communication systems [26]–[30]. Denoising CNN (DnCNN) [31] or fast and flexible denoising CNN (FFDNet) [32] were applied to estimate cell-free massive MIMO channels [26], visible light communication channels [27], intelligent reflecting surface (IRS)-assisted fading channels [28], [30], and ambient backscatter communication networks [29]. The studies have shown that the deep denoising networks reduce the channel estimation errors effectively. In particular, the FFDNet was favored in [26], [27], [30] owing to its robustness to different noise levels.

This paper considers channel estimation problems for a monostatic multiantenna BCN in a generalized fading model, where the backcatter MIMO channel is constructed by multiplying a correlated Rician fading vector and its transpose. In this case, the cascaded backcatter MIMO channel exhibits a complicated non-Gaussian distribution with which the optimal MMSE estimator is almost intractable as noted in another form of cascaded channels [29], [30]. This paper extends model-based suboptimal estimators proposed for backscatter and forward channels in [12] to fit in with a generalized channel model and explores deep learning solutions for a better performance. The major contributions of this paper are summarized as follows:

- We derive the LMMSE backscatter channel estimator in an explicit form by analyzing the statistics of the backscatter MIMO channel formed by cascading an identical spatially correlated Rician fading vector. This channel is more complicated than those of the cascaded channels formed by multiplying two independent Rayleigh fading channel vectors in [29], [30].
- To find a better solution, we apply the FFDNet [32] to denoise the LS backscatter channel estimate without knowing the channel statistics. In addition, we propose a modified FFDNet for an enhanced backscatter channel estimator by exploiting the symmetric property of the backscatter MIMO channel.
- Finally, we propose a DNN-based forward channel estimator which maps from the backscatter signal to the forward channel estimate directly and adopts a customized loss function designed by taking into account the sign ambiguity in estimation. The DNN-based forward channel estimator outperforms the model-based two-step channel estimators with a larger gain at less pilot overhead and more noisy channel.

Notation: The set of $n \times m$ complex-valued (real-valued) matrices is denoted by $\mathbb{C}^{n\times m}$ ($\mathbb{R}^{n\times m}$). The $n \times m$ matrix with all-zero (all-one) entries is denoted by $\mathbf{0}_{n\times m}$ ($\mathbf{1}_{n\times m}$). The $n \times n$ identity matrix is denoted by $\boldsymbol{I}_n$. We use $\mathrm{vec}(\boldsymbol{A})$, $\mathrm{tr}(\boldsymbol{A})$, $\|\boldsymbol{A}\|_F$, $\boldsymbol{A}^{-1}$, $\boldsymbol{A}^{\dagger}$, and $[\boldsymbol{A}]_{i,j}$ to denote the vectorization, trace, Frobenius norm, inverse, pseudo-inverse, and (i,j)th element of matrix $\boldsymbol{A}$, respectively. In addition, $\lambda_{\max}(\boldsymbol{A})$ denotes the maximum eigenvalue of matrix $\boldsymbol{A}$ and $\otimes$ denotes the Kronecker product of two matrices. We use $\Re\{\cdot\}$ and $\Im\{\cdot\}$ to denote the real and imaginary parts, respectively. We also use $\mathbb{E}[\cdot]$ for the expectation, $\mathcal{CN}(\boldsymbol{\mu}, \boldsymbol{\Lambda})$ for the complex Gaussian distribution with mean vector $\boldsymbol{\mu}$ and covariance matrix $\boldsymbol{\Lambda}$, and $\sim$ for "distributed as".

II. SYSTEM MODEL

Consider a monostatic BCN, where a multiantenna HAP serves single-antenna BDs as depicted in Fig. 1(a). The HAP equipped with M antennas operates in full-duplex; each antenna of the HAP excites a carrier signal and, simultaneously, receives a signal reflected by a BD. We assume the ideal full-duplex operation with perfect self-interference cancellation at the decoupler as in the other literature [8]–[17]. The forward channel from the HAP to the BD of our concern is described by $\sqrt{\omega}\boldsymbol{h}^T$, where ω denotes the path loss and $\boldsymbol{h} = [h_1, h_2, \cdots, h_M]^T$ represents the small-scale fading components subject to $\mathbb{E}[|h_m|^2] = 1$. The reverse channel from the BD to the HAP is given by $\sqrt{\omega}\boldsymbol{h}$ under the assumption that the channel reciprocity holds.

The small-scale fading is modeled by spatially correlated Rician fading as [33]

$$\boldsymbol{h} = \sqrt{\frac{K_o}{K_o+1}}\boldsymbol{h}_{\mathrm{LoS}} + \sqrt{\frac{1}{K_o+1}}\boldsymbol{h}_{\mathrm{NLoS}}, \tag{1}$$

This article has been accepted for publication in a future issue of this journal, but has not been fully edited. Content may change prior to final publication. Citation information: DOI 10.1109/ACCESS.2021.3134961, IEEE Access

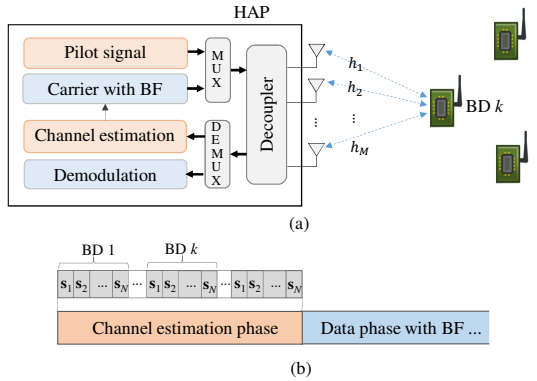

FIGURE 1. Full-duplex monostatic BCN with a multiantenna HAP and single-antenna BDs: (a) system model (b) frame structure.

where $\boldsymbol{h}_{\text{LoS}}$ represent the deterministic line-of-sight (LoS) component subject to $\|\boldsymbol{h}_{\text{LoS}}\|^2 = M$, $\boldsymbol{h}_{\text{NLoS}}$ denotes the random non-LoS (NLoS) one subject to $\mathbb{E}[\text{tr}(\boldsymbol{h}_{\text{NLoS}}\boldsymbol{h}_{\text{NLoS}}^H)] = M$, and K_o is the Rician factor reflecting the power fraction of the LoS to NLoS components. The channel in (1) can be rewritten as

$$\boldsymbol{h} = \boldsymbol{\mu}_{\boldsymbol{h}} + \tilde{\boldsymbol{h}} \sim \mathcal{CN}(\boldsymbol{\mu}_{\boldsymbol{h}}, \boldsymbol{C}_{\boldsymbol{h}}), \tag{2}$$

where $\boldsymbol{\mu}_{\boldsymbol{h}} = \sqrt{\frac{K_o}{K_o+1}}\boldsymbol{h}_{\text{LoS}}$, $\tilde{\boldsymbol{h}} = \sqrt{\frac{1}{K_o+1}}\boldsymbol{h}_{\text{NLoS}} \sim \mathcal{CN}(\boldsymbol{0}_{M\times 1}, \boldsymbol{C}_{\boldsymbol{h}})$, and $\boldsymbol{C}_{\boldsymbol{h}} = \mathbb{E}[(\boldsymbol{h} - \boldsymbol{\mu}_{\boldsymbol{h}})(\boldsymbol{h} - \boldsymbol{\mu}_{\boldsymbol{h}})^H]$ is the covariance matrix of $\boldsymbol{h}$. The channel is invariant over a time frame consisting of a channel estimation phase and a subsequent data phase shown in Fig. 1(b).

In the channel estimation phase, the HAP transmits N pilot symbols over M antennas for each BD at transmit power P. The transmit signal can be expressed as $\sqrt{P}\boldsymbol{s}_n$ for $n = 1, 2, \cdots, N$, where $\boldsymbol{s}_n \in \mathbb{C}^{M\times 1}$ is the pilot symbol vector subject to $\|\boldsymbol{s}_n\|^2 = 1$. The number of pilot symbols can be chosen as $N = M$ for full pilot overhead or as $N < M$ for reduced pilot overhead. The BD reflects the incident pilot signal $\sqrt{P\omega}\boldsymbol{h}^T\boldsymbol{s}_n$ with the reflection power coefficient $\beta_c \in (0, 1]$, which leads the received signal at the HAP as follows [9]–[17]:

$$\boldsymbol{r}_n = \sqrt{P\omega^2\beta_c}\boldsymbol{h}\boldsymbol{h}^T\boldsymbol{s}_n + \boldsymbol{z}_n \in \mathbb{C}^{M\times 1}, \tag{3}$$

where $\boldsymbol{z}_n \sim \mathcal{CN}(\boldsymbol{0}_{M\times 1}, \sigma_0^2\boldsymbol{I}_M)$ is the noise vector at the HAP with variance σ_0^2 for each component. We rewrite the received signal (3) in a matrix form after normalization as

$$\boldsymbol{Y} = \frac{1}{\sqrt{P\omega^2\beta_c}}[\boldsymbol{r}_1, \boldsymbol{r}_2, \cdots, \boldsymbol{r}_N] = \boldsymbol{G}\boldsymbol{S} + \boldsymbol{W}, \tag{4}$$

where $\boldsymbol{G} = \boldsymbol{h}\boldsymbol{h}^T \in \mathbb{C}^{M\times M}$ is the backscatter channel matrix, $\boldsymbol{S} = [\boldsymbol{s}_1, \boldsymbol{s}_2, \cdots, \boldsymbol{s}_N] \in \mathbb{C}^{M\times N}$ is the pilot symbol matrix, and $\boldsymbol{W} = [\boldsymbol{w}_1, \boldsymbol{w}_2, \cdots, \boldsymbol{w}_N] \in \mathbb{C}^{M\times N}$ with $\boldsymbol{w}_n = \frac{1}{\sqrt{P\omega^2\beta_c}}\boldsymbol{z}_n$ is the scaled noise matrix. Note that $\boldsymbol{w}_n \sim \mathcal{CN}(\boldsymbol{0}_{M\times 1}, \sigma^2\boldsymbol{I}_M)$, where the noise variance is given by the inverse of the end-to-end SNR $\gamma = \frac{P\omega^2\beta_c}{\sigma_0^2}$ as $\sigma^2 = 1/\gamma$.

As in [12], we construct the pilot signal matrix $\boldsymbol{S}$ with $N \times N$ orthogonal matrix $\boldsymbol{S}_N \in \mathbb{C}^{N\times N}$ as $\boldsymbol{S} = \boldsymbol{E}_N\boldsymbol{S}_N$, where $\boldsymbol{E}_N = [\boldsymbol{I}_N\ \boldsymbol{0}_{N\times(M-N)}]^T$. Without a loss of generality, we may set $\boldsymbol{S}_N = \boldsymbol{I}_N$ with which (4) becomes

$$\boldsymbol{Y} = \boldsymbol{G}_N + \boldsymbol{W}, \tag{5}$$

where

$$\boldsymbol{G}_N = \boldsymbol{G}\boldsymbol{E}_N = \begin{bmatrix} h_1^2 & h_1h_2 & \cdots & h_1h_N \\ h_2h_1 & h_2^2 & \cdots & h_2h_N \\ \vdots & \vdots & \ddots & \vdots \\ h_Mh_1 & h_Mh_2 & \cdots & h_Mh_N \end{bmatrix}. \tag{6}$$

corresponds to the $M \times N$ submatrix of $\boldsymbol{G}$. In [12], [14], [15], the truncated backscatter channel $\boldsymbol{G}_N$ was estimated through the LS and LMMSE criteria when the forward channel undergoes uncorrelated Rayleigh fading as $\boldsymbol{h} \sim \mathcal{CN}(\boldsymbol{0}_{M\times 1}, \boldsymbol{I}_M)$. The forward channel $\boldsymbol{h}$ was also estimated from $\hat{\boldsymbol{G}}_N$ through EVD and additional decorrelation for reduced pilot overhead in [12].

We generalize the model-based channel estimators [12], [14], [15] to be fitted into the correlated Rician fading. We then propose learning-based estimators for both backsatter and forward channels to improve the performance through denoising and unified approximation.

III. BACKSCATTER CHANNEL ESTIMATION

This section provides model-based and learning-based backscatter channel estimators in the generalized channel model.

A. MODEL-BASED ESTIMATION

The optimal MMSE estimator of $\boldsymbol{G}_N$ from the observation (5) is given by the conditional expectation as [34]

$$\hat{\boldsymbol{G}}_N^{mmse} = \mathbb{E}[\boldsymbol{G}_N|\boldsymbol{Y}]. \tag{7}$$

The entries of the backscatter channel $\boldsymbol{G}_N$ as shown in (6) are multiplications of two correlated complex Gaussian random variables that are not Gaussian anymore. Thus, the conditional distribution of $\boldsymbol{G}_N$ given $\boldsymbol{Y}$ is intricate to derive and so is the optimal MMSE estimator. Instead, we consider suboptimal linear estimators in the generalized fading.

The LS estimator that is independent of the channel statistics can be applicable to any fading model. With (5), the LS estimator of $\boldsymbol{G}_N$ is simply given by

$$\hat{\boldsymbol{G}}_N^{ls} = \arg\min_{\boldsymbol{G}_N} \|\boldsymbol{Y} - \boldsymbol{G}_N\|_F = \boldsymbol{Y} \tag{8}$$

that leads to the MSE

$$\text{MSE}_{\hat{\boldsymbol{G}}_N^{ls}} = \mathbb{E}[\|\boldsymbol{G}_N - \boldsymbol{G}_N^{ls}\|_F^2] = MN\sigma^2. \tag{9}$$

The LMMSE estimator of $\boldsymbol{G}_N$ depending on the channel statistics can be derived by analyzing the first and second statistics of the backscatter channel in a vector form. For this purpose, let us express the received signal in a vector form as

$$\mathbf{y} = \text{vec}(\boldsymbol{Y}) = \mathbf{g}_N + \mathbf{w}, \tag{10}$$

This article has been accepted for publication in a future issue of this journal, but has not been fully edited. Content may change prior to final publication. Citation information: DOI 10.1109/ACCESS.2021.3134961, IEEE Access

where $\mathbf{g}_N = \text{vec}(\boldsymbol{G}_N)$ and $\mathbf{w} = \text{vec}(\boldsymbol{W}) \sim \mathcal{CN}(\mathbf{0}_{MN\times 1}, \sigma^2 \boldsymbol{I}_{MN})$. The LMMSE backscatter channel estimator of $\mathbf{g}_N$ is then expressed as [34]

$$\hat{\mathbf{g}}_N^{lm} = \boldsymbol{\mu}_{\mathbf{g}_N} + \boldsymbol{C}_{\mathbf{g}_N}(\boldsymbol{C}_{\mathbf{g}_N} + \sigma^2 \boldsymbol{I}_{MN})^{-1}(\mathbf{y} - \boldsymbol{\mu}_{\mathbf{g}_N}), \quad (11)$$

where $\boldsymbol{\mu}_{\mathbf{g}_N} = \mathbb{E}[\mathbf{g}_N]$ and $\boldsymbol{C}_{\mathbf{g}_N} = \mathbb{E}[(\mathbf{g}_N - \boldsymbol{\mu}_{\mathbf{g}_N})(\mathbf{g}_N - \boldsymbol{\mu}_{\mathbf{g}_N})^H]$. The MSE of the LMMSE estimator (11) is also given by

$$\text{MSE}_{\hat{\mathbf{g}}_N^{lm}} = \text{tr}\left(\left(\boldsymbol{C}_{\mathbf{g}_N}^{\dagger} + \tfrac{1}{\sigma^2}\boldsymbol{I}_{MN}\right)^{-1}\right), \quad (12)$$

which is the minimum MSE value among the linear backscatter channel estimators.

For the analytical expression of (11) and (12), we obtain $\boldsymbol{\mu}_{\mathbf{g}_N}$ and $\boldsymbol{C}_{\mathbf{g}_N}$ by taking the $MN \times 1$ subvector of $\boldsymbol{\mu}_{\mathbf{g}}$ and $NM \times NM$ submatrix of $\boldsymbol{C}_{\mathbf{g}}$, respectively, where the mean vector $\boldsymbol{\mu}_{\mathbf{g}}$ and covariance matrix $\boldsymbol{C}_{\mathbf{g}}$ of $\mathbf{g} = \text{vec}(\boldsymbol{h}\boldsymbol{h}^T)$ are derived in explicit forms in Appendix A as follows:

$$\boldsymbol{\mu}_{\mathbf{g}} = \text{vec}(\boldsymbol{\mu}_{\boldsymbol{h}}\boldsymbol{\mu}_{\boldsymbol{h}}^T) \quad (13)$$

and

$$\begin{aligned}\boldsymbol{C}_{\mathbf{g}} = {} & \mathfrak{M}_{\boldsymbol{h}} \otimes \boldsymbol{C}_{\boldsymbol{h}} + \boldsymbol{C}_{\boldsymbol{h}} \otimes \mathfrak{M}_{\boldsymbol{h}} + \boldsymbol{C}_{\boldsymbol{h}} \otimes \boldsymbol{C}_{\boldsymbol{h}} \\ & + \boldsymbol{T}_{M^2}[\mathfrak{M}_{\boldsymbol{h}} \otimes \boldsymbol{C}_{\boldsymbol{h}} + \boldsymbol{C}_{\boldsymbol{h}} \otimes \mathfrak{M}_{\boldsymbol{h}} + \boldsymbol{C}_{\boldsymbol{h}} \otimes \boldsymbol{C}_{\boldsymbol{h}}], \quad (14)\end{aligned}$$

where $\mathfrak{M}_{\boldsymbol{h}} = \boldsymbol{\mu}_{\boldsymbol{h}}\boldsymbol{\mu}_{\boldsymbol{h}}^H$, $\otimes$ denotes the Kronecker product, and $\boldsymbol{T}_{M^2}$ is the $M^2 \times M^2$ communication matrix having one at the $((p-1)M+q, (q-1)M+p)$th entry for $p, q \in \mathcal{M} \triangleq \{1, 2, \cdots, M\}$ while having zero elsewhere. In a special case of a correlated Rayleigh fading with $K_o = 0$, we have $\boldsymbol{\mu}_{\mathbf{g}} = \mathbf{0}_{M^2}$ and

$$\boldsymbol{C}_{\mathbf{g}} = (\boldsymbol{I}_{M^2} + \boldsymbol{T}_{M^2})(\boldsymbol{C}_{\boldsymbol{h}} \otimes \boldsymbol{C}_{\boldsymbol{h}}). \quad (15)$$

B. LEARNING-BASED ESTIMATION

As an attempt to find a backscatter channel estimator closer to the optimal one, we apply the FFDNet [32] used for image denoising by regarding the backscatter channel $\boldsymbol{G}_N$ as a two-dimensional image. The FFDNet is a CNN-based denoising architecture to be made robust to different noise levels and has been applied to the channel estimation problems successfully [26], [27], [30]. Motivated by these recent works, we apply the existing FFDNet architecture directly to backscatter channel estimation and look for a more appropriate adaptation of the FFDNet to the symmetric backscatter channel.

Fig. 2(a) illustrates the FFDNet architecture applied to the backscatter channel estimator directly. The FFDNet inputs the received signal $\boldsymbol{Y} = \boldsymbol{G}_N + \boldsymbol{W}$ (equivalent to the LS estimate of $\boldsymbol{G}_N$) and outputs the denoised backscatter channel estimator $\hat{\boldsymbol{G}}_N^{\mathcal{F}}$. The input $\boldsymbol{Y}$ is first expressed in a real-valued tensor of size $M \times N \times 2$ by arranging the real and imaginary parts of the $M \times N$ complex entries and is then reshaped through downsampling into a tensor $\mathcal{Y}$ of size $\frac{M}{2} \times N \times 4$ to create four channels to comply with the FFDNet input [32]. Additionally, a noise level map $\boldsymbol{\Sigma}$ of size $\frac{M}{2} \times N$ is input to the FFDNet, where $[\boldsymbol{\Sigma}]_{m,n} = \frac{\sigma}{\sqrt{2}}$ represents the standard deviation of the noise in $[\mathcal{Y}]_{m,n,c}$ which is assumed to be

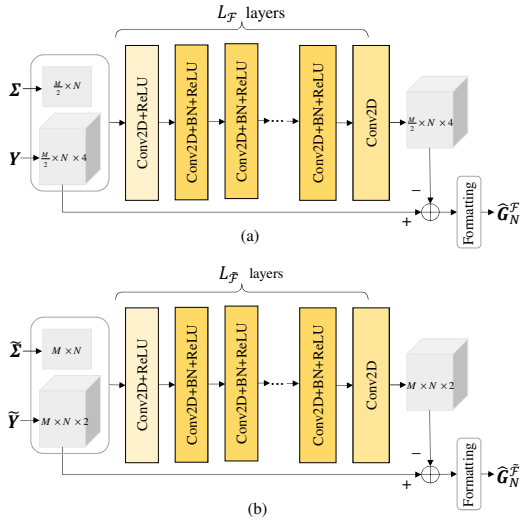

FIGURE 2. CNN-based denoising architectures for backscatter channel estimation: (a) FFDNet (b) mFFDNet.

identical for $c = 1, 2, 3, 4$. Hence, the size of the input tensor is given by $\frac{M}{2} \times N \times 5$. The FFDNet with depth $L_{\mathcal{F}}$ processes the input tensor through a number of convolutional layers; the first layer consists of convolution operation (Conv2D) and rectified linear unit (ReLU) activation, each layer of the subsequent $L_{\mathcal{F}} - 2$ layers consists of Conv2D, batch normalization (BN), and ReLU activation, and the last layer consists of Conv2D only. Conv2D is performed with a filter of kernel size $(s_l \times s_l) = (3 \times 3)$ along with zero-padding to keep the dimension $\frac{M}{2} \times N$ of each feature. The number of output feature maps is set to be equal as $f_l = F$ for $l = 1, 2, \cdots, L_{\mathcal{F}} - 1$ while that of the last layer is given by $f_{L_{\mathcal{F}}} = 4$ to comply with the output dimensions.

The backscatter channel estimator obtained with the FFDNet as in Fig. 2(a) can be expressed as[1]

$$\hat{\boldsymbol{G}}_N^{\mathcal{F}} = \mathcal{F}(\boldsymbol{Y}, \boldsymbol{\Sigma}; \boldsymbol{\Theta}_{\mathcal{F}}), \quad (16)$$

where $\boldsymbol{\Theta}_{\mathcal{F}}$ denotes the set of the FFDNet parameters to be optimized during the training. With a labelled train data set $\{(\boldsymbol{Y}^{(k)}, \boldsymbol{\Sigma}^{(k)}, \boldsymbol{G}_N^{(k)})\}_{k=1}^{K_{\mathcal{F}}}$ of $K_{\mathcal{F}}$ samples, the FFDNet is trained offline to minimize the MSE loss function

$$\mathcal{L}_{\mathcal{F}}(\boldsymbol{\Theta}_{\mathcal{F}}) = \frac{1}{K_{\mathcal{F}}} \sum_{k=1}^{K_{\mathcal{F}}} \|\mathcal{F}(\boldsymbol{Y}^{(k)}, \boldsymbol{\Sigma}^{(k)}; \boldsymbol{\Theta}_{\mathcal{F}}) - \boldsymbol{G}_N^{(k)}\|_F^2. \quad (17)$$

We next adapt the input and architecture of the FFDNet as shown in Fig. 2(b), referred to as the modified FFDNet (mFFDNet) in sequel, to exploit the symmetry property of the backscatter channel; unlike the IRS channel constructed by cascading two independent channel vectors, the backscatter channel constructed as $\boldsymbol{G} = \boldsymbol{h}\boldsymbol{h}^T$ satisfies the symmetry condition of $\boldsymbol{G} = \boldsymbol{G}^T$. For the enhanced input, we obtain

[1]The complex-valued mathematical expressions $\boldsymbol{Y}$ and $\hat{\boldsymbol{G}}_N$ are used for the input and output of the FFDNet given in tensor forms without a loss of generality.

This article has been accepted for publication in a future issue of this journal, but has not been fully edited. Content may change prior to final publication. Citation information: DOI 10.1109/ACCESS.2021.3134961, IEEE Access

the symmetrically averaged LS estimator $\tilde{\boldsymbol{Y}}$ from the LS estimator $\boldsymbol{Y}$ of $\boldsymbol{G}_N$ as

$$\tilde{\boldsymbol{Y}} = \Phi_a(\boldsymbol{Y}), \tag{18}$$

where $\Phi_a(\cdot)$ denotes the symmetric average operation defined as

$$\Phi_a(\boldsymbol{X}) = \tfrac{1}{2}(\boldsymbol{X} + \boldsymbol{X}^T) \tag{19}$$

for $\boldsymbol{X} \in \mathbb{C}^{M\times M}$ and as

$$[\Phi_a(\boldsymbol{X})]_{mn} = \begin{cases} \frac{1}{2}([\boldsymbol{X}]_{mn} + [\boldsymbol{X}]_{nm}), & 1 \le m, n \le N \\ [\boldsymbol{X}]_{mn}, & m > N, n = 1, 2, \cdots, N \end{cases} \tag{20}$$

for $\boldsymbol{X} \in \mathbb{C}^{M\times N}$ with $N < M$. Equivalently, we can express (18) as

$$\tilde{\boldsymbol{Y}} = \boldsymbol{G}_N + \tilde{\boldsymbol{W}}, \tag{21}$$

where the (m, n)th entry of the symmetrically averaged noise matrix $\tilde{\boldsymbol{W}}$ is given by

$$\tilde{\sigma}^2_{mn} = \begin{cases} \frac{1}{2}\sigma^2, & m \ne n, m, n = 1, 2, \cdots, N, \\ \sigma^2, & \text{otherwise.} \end{cases} \tag{22}$$

We rearrange $\tilde{\boldsymbol{Y}}$ into a tensor of size $M \times N \times 2$ with two $M \times N$ matrices for the real and imaginary parts of $\tilde{\boldsymbol{Y}}$. The $M \times N$ noise map $\tilde{\boldsymbol{\Sigma}}$ for $\tilde{\boldsymbol{Y}}$ is constructed as $[\tilde{\boldsymbol{\Sigma}}]_{mn} = \frac{1}{\sqrt{2}}\tilde{\sigma}_{mn}$. Thus, $(\tilde{\boldsymbol{Y}}, \tilde{\boldsymbol{\Sigma}})$ in a tensor of size $M\times N\times 3$ serves as the input for the mFFDNet. The mFFDNet of depth $L_{\tilde{\mathcal{F}}}$ is constructed in a similar way as the FFDNet except for the first layer having the input tensor of size $M \times N \times 3$ and the last layer having $f_{L_{\tilde{\mathcal{F}}}} = 2$ output feature maps to comply with the output dimensions.

The backscatter channel estimator obtained with the mFFDNet described in Fig. 2(b) is expressed as

$$\hat{\boldsymbol{G}}_N^{\tilde{\mathcal{F}}} = \tilde{\mathcal{F}}(\tilde{\boldsymbol{Y}}, \tilde{\boldsymbol{\Sigma}}; \boldsymbol{\Theta}_{\tilde{\mathcal{F}}}), \tag{23}$$

where $\boldsymbol{\Theta}_{\tilde{\mathcal{F}}}$ denotes the set of the mFFDNet parameters to be optimized during the training. With a labelled train data set $\{(\tilde{\boldsymbol{Y}}^{(k)}, \tilde{\boldsymbol{\Sigma}}^{(k)}, \boldsymbol{G}_N^{(k)})\}_{k=1}^{K_{\tilde{\mathcal{F}}}}$, the mFFDNet is trained to minimize the MSE loss function

$$\mathcal{L}_{\tilde{\mathcal{F}}}(\boldsymbol{\Theta}_{\tilde{\mathcal{F}}}) = \frac{1}{K_{\tilde{\mathcal{F}}}} \sum_{k=1}^{K_{\tilde{\mathcal{F}}}} \|\boldsymbol{G}_N^{(k)} - \Phi_a(\hat{\boldsymbol{G}}_N^{\tilde{\mathcal{F}},(k)})\|_F^2 \tag{24}$$

with $\hat{\boldsymbol{G}}_N^{\tilde{\mathcal{F}},(k)} = \tilde{\mathcal{F}}(\tilde{\boldsymbol{Y}}^{(k)}, \tilde{\boldsymbol{\Sigma}}^{(k)}; \boldsymbol{\Theta}_{\tilde{\mathcal{F}}})$.

The trained network, $\boldsymbol{\Theta}^\star_{\mathcal{F}}$ for the FFDNet or $\boldsymbol{\Theta}^\star_{\tilde{\mathcal{F}}}$ for the mFFDNet, is implemented at the HAP to estimate the backscatter channel online in practice.

A time complexity of a CNN-based network was computed as [35]

$$\mathcal{O}\left(\sum_{l=1}^{L} n_{h,l} n_{w,l} f_{l-1} s_l^2 f_l\right) \tag{25}$$

where L is the number of convolution layers, $n_{w,l}$ and $n_{h,l}$ are the width and height of the lth layer, s_l^2 is the kernel size, and f_{l-1} and f_l are the number of input and output feature maps (channels), respectively. The time complexity of the FFDNet and mFFDNet backscatter channel estimators is thus given by

$$C_{\mathcal{F}} = \mathcal{O}(4.5MN(9F + (L_{\mathcal{F}} - 2)F^2)) \tag{26}$$

and

$$C_{\tilde{\mathcal{F}}} = \mathcal{O}(9MN(5F + (L_{\tilde{\mathcal{F}}} - 2)F^2)), \tag{27}$$

respectively, where the complexity of the mFFDNet is twice that of the FFDNet when $L_{\mathcal{F}} = L_{\tilde{\mathcal{F}}}$ and the other conditions are the same.

IV. FORWARD CHANNEL ESTIMATION

This section presents a model-based forward channel estimator using a backscatter channel estimate and proposes a learning-based forward channel estimator mapping a received signal to a forward channel estimate directly.

A. MODEL-BASED ESTIMATION

We first summarize the model-based forward channel estimator $\hat{\boldsymbol{h}}$ derived from a backscatter channel estimate $\hat{\boldsymbol{G}}_N$ proposed in [12]. The estimator does not depend on the channel statistics so that it can be applied in the generalized fading channel model.

Let us express the forward channel vector as $\boldsymbol{h} = [\boldsymbol{h}_{\mathcal{A}}^T \ \boldsymbol{h}_{\mathcal{B}}^T]^T$, where $\boldsymbol{h}_{\mathcal{A}} = [h_1, h_2, \cdots, h_N]^T$ and $\boldsymbol{h}_{\mathcal{B}} = [h_{N+1}, h_{N+2}, \cdots, h_M]^T$; note that $\boldsymbol{h}_{\mathcal{A}} = \boldsymbol{h}$ if $N = M$. The backscatter channel is then expressed as

$$\boldsymbol{G}_N = \begin{bmatrix} \boldsymbol{h}_{\mathcal{A}} \\ \boldsymbol{h}_{\mathcal{B}} \end{bmatrix} \boldsymbol{h}_{\mathcal{A}}^T = \begin{bmatrix} \boldsymbol{Q}_{\mathcal{A}} \\ \boldsymbol{Q}_{\mathcal{B}} \end{bmatrix}, \tag{28}$$

where $\boldsymbol{Q}_{\mathcal{A}} = \boldsymbol{h}_{\mathcal{A}}\boldsymbol{h}_{\mathcal{A}}^T$ and $\boldsymbol{Q}_{\mathcal{B}} = \boldsymbol{h}_{\mathcal{B}}\boldsymbol{h}_{\mathcal{A}}^T$. From the properties

$$\boldsymbol{Q}_{\mathcal{A}}\boldsymbol{h}_{\mathcal{A}}^* = \|\boldsymbol{h}_{\mathcal{A}}\|^2\boldsymbol{h}_{\mathcal{A}}, \tag{29}$$

$$\boldsymbol{Q}_{\mathcal{B}}\boldsymbol{h}_{\mathcal{A}}^* = \|\boldsymbol{h}_{\mathcal{A}}\|^2\boldsymbol{h}_{\mathcal{B}}, \tag{30}$$

we estimate $\hat{\boldsymbol{h}}_{\mathcal{A}}$ and $\hat{\boldsymbol{h}}_{\mathcal{B}}$ from an estimate $\hat{\boldsymbol{G}}_N \triangleq [\hat{\boldsymbol{Q}}_{\mathcal{A}}^T \ \hat{\boldsymbol{Q}}_{\mathcal{B}}^T]^T$ obtained in the previous section as follows. Firstly, we note from (29) that

$$\underbrace{\begin{bmatrix} \Re\{\boldsymbol{Q}_{\mathcal{A}}\} & \Im\{\boldsymbol{Q}_{\mathcal{A}}\} \\ \Im\{\boldsymbol{Q}_{\mathcal{A}}\} & -\Re\{\boldsymbol{Q}_{\mathcal{A}}\} \end{bmatrix}}_{\triangleq \mathbf{Q}_{\mathcal{A}}} \underbrace{\begin{bmatrix} \Re\{\boldsymbol{h}_{\mathcal{A}}\} \\ \Im\{\boldsymbol{h}_{\mathcal{A}}\} \end{bmatrix}}_{\triangleq \mathbf{h}_{\mathcal{A}}} = \|\boldsymbol{h}_{\mathcal{A}}\|^2 \begin{bmatrix} \Re\{\boldsymbol{h}_{\mathcal{A}}\} \\ \Im\{\boldsymbol{h}_{\mathcal{A}}\} \end{bmatrix}, \tag{31}$$

where $\mathbf{h}_{\mathcal{A}}$ is the eigenvector of $\mathbf{Q}_{\mathcal{A}}$ leading to the maximum positive eigenvalue. Thus, we obtain $\hat{\boldsymbol{h}}_{\mathcal{A}}$ by finding the eigenvector leading to the maximum eigenvalue of $\hat{\mathbf{Q}}_{\mathcal{A}}$ constructed with $\hat{\boldsymbol{Q}}_{\mathcal{A}}$. From (30), we next obtain $\hat{\boldsymbol{h}}_{\mathcal{B}}$ with $\hat{\boldsymbol{h}}_{\mathcal{A}}$ as follows:

$$\hat{\boldsymbol{h}}_{\mathcal{B}} = \frac{\hat{\boldsymbol{Q}}_{\mathcal{B}}\hat{\boldsymbol{h}}_{\mathcal{A}}^*}{\|\hat{\boldsymbol{h}}_{\mathcal{A}}\|^2}. \tag{32}$$

Remark 1: If the HAP transmits the full pilot symbols as $N = M$, we only need to estimate $\boldsymbol{h} = \boldsymbol{h}_{\mathcal{A}}$ through EVD.

Remark 2: If the HAP transmits $N < M$ pilot symbols for reduced overhead, the quality of $\hat{\boldsymbol{h}}_{\mathcal{A}}$ would affect the performance of $\hat{\boldsymbol{h}}_{\mathcal{B}}$.

This article has been accepted for publication in a future issue of this journal, but has not been fully edited. Content may change prior to final publication. Citation information: DOI 10.1109/ACCESS.2021.3134961, IEEE Access

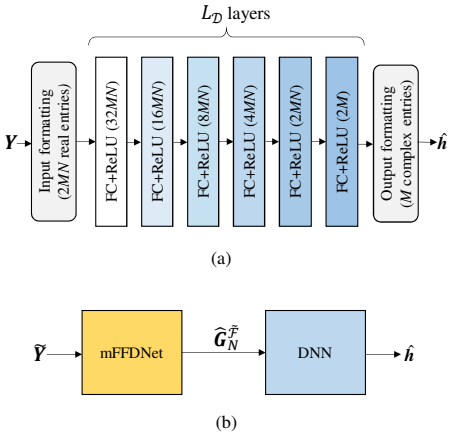

FIGURE 3. DNN-based forward channel estimation; (a) DNN architecture (b) two-step estimation assisted by mFFDNet.

B. LEARNING-BASED ESTIMATION

This subsection provides a DNN-based forward channel estimator that maps a received signal $\boldsymbol{Y}$ to an estimate $\hat{\boldsymbol{h}}$ directly without estimating $\hat{\boldsymbol{G}}_N$. The method not only avoids error propagation incurred with reduced pilot overhead but also removes additional estimation of $\boldsymbol{G}_N$ with channel statistics or deep learning techniques.

Fig. 3(a) illustrates the DNN architecture accepting $\boldsymbol{Y}$ for the input [2] and producing $\hat{\boldsymbol{h}}$ for the output. The DNN is implemented with real-valued input vector $[\Re\{\mathbf{y}\}^T \ \Re\{\mathbf{y}\}^T]^T$ of length $2MN$ and real-valued output vector $[\Re\{\hat{\boldsymbol{h}}\}^T \ \Re\{\hat{\boldsymbol{h}}\}^T]^T$ of length $2M$. The DNN with depth $L_{\mathcal{D}}$ is constructed with $L_{\mathcal{D}}-1$ fully-connected (FC) hidden layers with ReLU activation and the output layer with the linear activation. The number of neurons at each hidden layer is proportional to the input dimension. The input and output relationship is described with complex-valued notation used for model-based estimation as

$$\hat{\boldsymbol{h}} = \mathcal{D}(\boldsymbol{Y}; \boldsymbol{\Theta}_{\mathcal{D}}), \tag{33}$$

where $\boldsymbol{\Theta}_{\mathcal{D}}$ represents the set of all parameters of the DNN performing forward channel estimation.

The loss function for the DNN-based forward channel estimator is designed by taking into account the sign ambiguity of the forward channel estimate obtained from the backscatter channel; the sign information of $\boldsymbol{h}$ can not be recovered from $\hat{\boldsymbol{G}}_N$ since both $\boldsymbol{h}$ and $-\boldsymbol{h}$ lead to the same backscatter channel $\boldsymbol{G} = \boldsymbol{h}\boldsymbol{h}^T$ (or equivalently $\boldsymbol{G}_N$). In this regard, we define unsigned square error (USE) as

$$\text{USE}(\boldsymbol{h}, \hat{\boldsymbol{h}}) = \min(||\boldsymbol{h} - \hat{\boldsymbol{h}}||^2, ||\boldsymbol{h} + \hat{\boldsymbol{h}}||^2) \tag{34}$$

which is used for a customized loss function. For a training data set $\{(\boldsymbol{Y}^{(k)}, \boldsymbol{h}^{(k)})\}_{k=1}^{K_{\mathcal{D}}}$ with $K_{\mathcal{D}}$ samples, the mean USE (MUSE) loss function is computed as

$$\mathcal{L}_{\mathcal{D}}(\boldsymbol{\Theta}_{\mathcal{D}}) = \frac{1}{K_{\mathcal{D}}} \sum_{k=1}^{K_{\mathcal{D}}} \text{USE}(\boldsymbol{h}^{(k)}, \mathcal{D}(\boldsymbol{Y}^{(k)}; \boldsymbol{\Theta}_{\mathcal{D}})) \tag{35}$$

[2]We use $\boldsymbol{Y}$ instead of $\tilde{\boldsymbol{Y}}$ since both inputs provide indistinguishable performances that will be shown in performance evaluation.

that is minimized during the training process performed offline. The optimized DNN $\boldsymbol{\Theta}_{\mathcal{D}}^{\star}$ is then implemented at the HAP for online forward channel estimation.

To see any possibility of performance improvement, we may consider a two-step forward channel estimation by concatenating the mFFDNet proposed for backscatter channel estimation with the DNN for forward channel estimation as in Fig. 3(b). In this case, the DNN is trained with the output of the mFFDNet as $\{(\hat{\boldsymbol{G}}_N^{\mathcal{F},(k)}, \boldsymbol{h}^{(k)})\}_{k=1}^{K_{\mathcal{D}}}$.

V. PERFORMANCE EVALUATION

This section evaluates the performance of the proposed channel estimators in correlated Rayleigh and Rician fading. For Rician fading, the LoS component is set to $\boldsymbol{h}_{\text{LoS}} = \sqrt{M}\boldsymbol{a}(\theta_0)$, where

$$\boldsymbol{a}(\theta) = \frac{1}{\sqrt{M}}[1, e^{-j\frac{2\pi d}{\lambda}\sin(\theta)}, \cdots, e^{-j\frac{2\pi(M-1)d}{\lambda}\sin(\theta)}]^T \tag{36}$$

is the antenna array response vector of the uniform linear array with antenna spacing d, wavelength λ, and departure angle θ [23]. We set $d = \lambda/2$ and $\theta_0 = 73°$ in the following results. The covariance matrix of the NLoS component is parameterized by correlation coefficient ρ as $[\boldsymbol{C}_{\boldsymbol{h}}]_{i,j} = \frac{1}{K_o+1}\rho^{|i-j|}$ for $i, j \in \mathcal{M}$. The performance is evaluated in terms of the average end-to-end SNR at the HAP defined in Section II as $\gamma = \frac{1}{\sigma^2} = \frac{P\omega^2\beta_c}{\sigma_0^2}$.

A. BACKSCATTER CHANNEL ESTIMATION

We first provides the performance of the backscatter channel estimators designed with mathematical model and deep learning. For deep learning with FFDNet and mFFDNet, we set the depth to $L_{\mathcal{F}} = L_{\tilde{\mathcal{F}}} = 15$ and the number of output feature maps to $F = 64$. In addition, $300,000$, $100,000$, and $100,000$ data samples are used for training, validation, and test, respectively. The FDDNet and mFFDNet are optimized through the ADAM optimizer with learning rate 0.001 and mini-batch size 500. The training process lasts up to 100 epochs with patience in 10 epochs.

The performance of the backscatter channel estimators is shown in Fig. 4 in terms of the normalized MSE, $\frac{1}{MN}\mathbb{E}[\|\hat{\boldsymbol{G}}_N - \boldsymbol{G}_N\|_F^2]$, when the forward channel undergoes Rayleigh fading ($K_o = 0$) with correlation $\rho = 0.8$. For $M = 8$ antennas at the HAP, the number of pilot symbols is set to $N = 8$ for full pilot overhead in Fig. 4(a) and $N = 2$ for reduced pilot overhead in Fig. 4(b). Due to the correlation in the backscatter channel, a large gain of the LMMSE over LS estimator is observed in the low SNR region. In addition, learning-based estimators using FFDNet and mFFDNet outperform the LMMSE estimator toward the optimal MMSE. The mFFDNet provides the best performance using the noise-reduced input $\tilde{\boldsymbol{Y}}$ instead of $\boldsymbol{Y}$ when $M = N = 8$ in Fig. 4(a), where the symmetric averaging operation is the most effective with $\tilde{\boldsymbol{Y}} = \frac{1}{2}(\boldsymbol{Y} + \boldsymbol{Y}^T)$. When the number of pilots is reduced to $N = 2$ in Fig. 4(b), the normalized MSE of $\hat{\boldsymbol{G}}_N$ increases since the number of observation data is reduced from $8M$ to $2M$. The gain of mFFDNet over

This article has been accepted for publication in a future issue of this journal, but has not been fully edited. Content may change prior to final publication. Citation information: DOI 10.1109/ACCESS.2021.3134961, IEEE Access

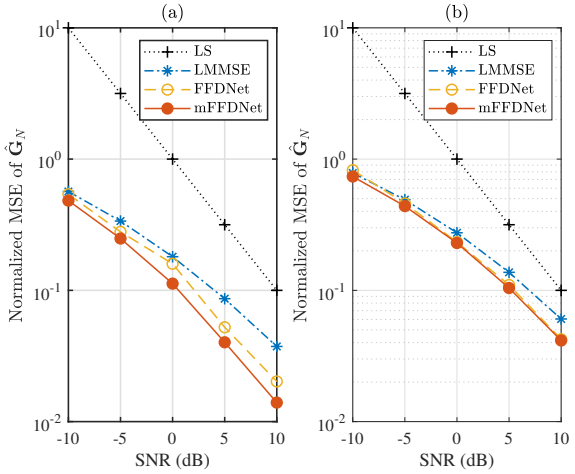

FIGURE 4. Normalized MSE of the backscatter channel estimators in Rayleigh fading with $K_o = 0$ and $\rho = 0.8$: (a) $(M, N) = (8, 8)$ (b) $(M, N) = (8, 2)$.

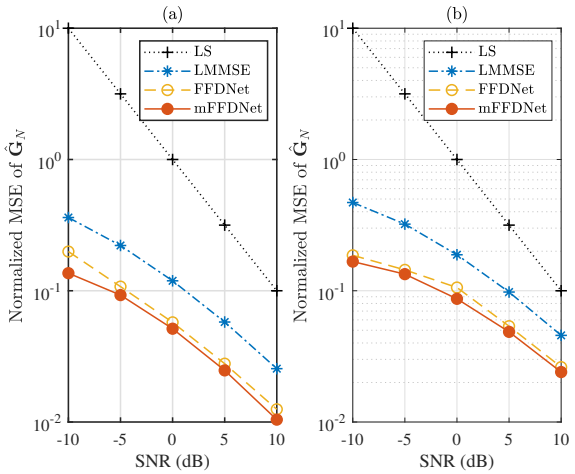

FIGURE 5. Normalized MSE of the backscatter channel estimators in Rician fading with $K_o = 2$ and $\rho = 0.8$: (a) $(M, N) = (8, 8)$ (b) $(M, N) = (8, 2)$.

FFDNet is negligible since only two components in $\boldsymbol{G}_N$ are symmetric.

The normalized MSE of $\hat{\boldsymbol{G}}_N$ in Rician fading with $K_o = 2$ and $\rho = 0.8$ is also shown in Fig. 5 with the other conditions remaining unchanged from Fig. 4. As the Rician factor increases from $K_o = 0$ in Fig. 4 to $K_o = 2$ in Fig. 5, the performance of the LMMSE and learning-based estimators gets improved due to the reduced randomness in the Rician fading. The gain of a learning-based estimator over the LMMSE one becomes larger as the Rician factor K_o increases. In particular, the improvement is more significant in the low SNR region and with reduced pilot overhead since the LoS component common to all the observed data can help reduce the noise during the training process.

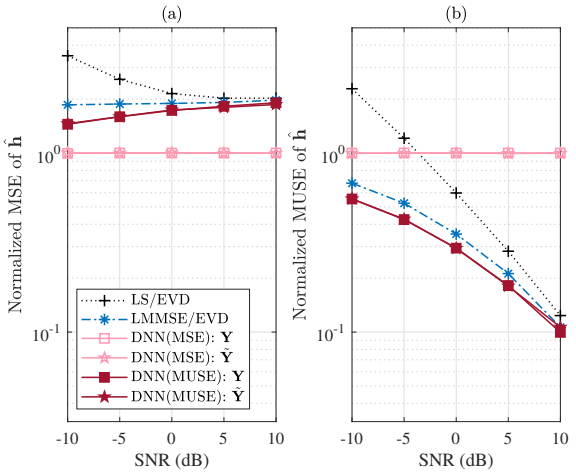

FIGURE 6. Performance of the forward channel estimators in Rayleigh fading channel with $K_o = 0$ and $\rho = 0.8$ when $M = 8$ and $N = 2$: (a) Normalized MSE (b) Normalized MUSE.

B. PERFORMANCE OF FORWARD CHANNEL ESTIMATION

This subsection provides the performance of the model- and learning-based forward channel estimators in the generalized fading channel. For the DNN-based estimator, we construct the network with depth $L_{\mathcal{D}} = 6$ and generate $300,000$, $100,000$, and $100,000$, samples for training, validation, and test respectively. The DNN is trained using the ADAM optimizer with learning rate 0.0002 and mini-batch size 128. The mFFDNet, if applied, is trained as delineated in the previous subsection.

We first investigate the validity of the new metric for forward channel estimation in Fig. 6 under Rayleigh fading with $K_o = 0$ and $\rho = 0$ when $M = 8$ and $N = 2$. Fig. 6(a) provides the normalized MSE $\frac{1}{M}\mathbb{E}[\|\boldsymbol{h} - \hat{\boldsymbol{h}}\|^2]$ adopted in [12], [14] whilst Fig. 6(b) provides the normalized MUSE $\frac{1}{M}\mathbb{E}[\text{USE}(\boldsymbol{h}, \hat{\boldsymbol{h}})]$ as the average SNR γ increases. In the figures, LS/EVD and LMMSE/EVD denote the model-based forward channel estimator described in Subsection IV-A using LS and LMMSE estimates for $\hat{\boldsymbol{G}}_N$ while DNN(MUSE) and DNN(MSE) denote the DNN-based estimators employing MUSE and MSE for the loss function, respectively. For the DNN-based estimators, we also consider two possible input $\boldsymbol{Y}$ and $\tilde{\boldsymbol{Y}}$ which leads to almost the same results. Although the traditional MSE fails to unveil a performance improvement as the SNR increases in Fig. 6(a), the proposed MUSE reveals the improvement in Fig. 6(b). The DNN with the MSE loss function is not trained in both MSE and MUSE. However, the DNN with MUSE loss function has been trained successfully to provide an improvement over the LMMSE/EVD in MUSE. Thus, in the following results, we use the normalized MUSE for the performance metric of the forward channel estimators.

We next compare the normalized MUSE of $\hat{\boldsymbol{h}}$ obtained with the model-based and learning-based estimators in Fig. 7 under the same configurations of Fig. 5; $(M, N) = (8, 8)$

This article has been accepted for publication in a future issue of this journal, but has not been fully edited. Content may change prior to final publication. Citation information: DOI 10.1109/ACCESS.2021.3134961, IEEE Access

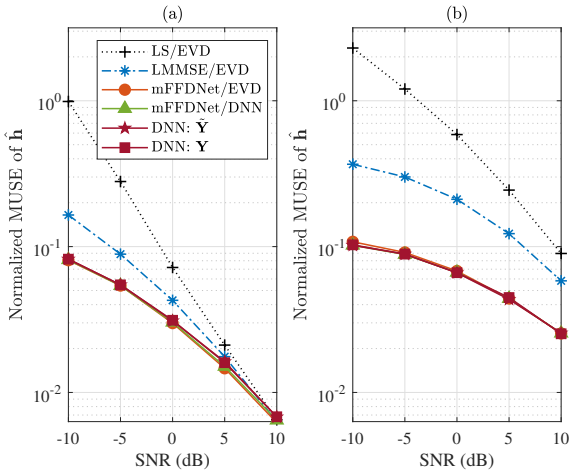

FIGURE 7. Normalized MUSE of $\hat{\boldsymbol{h}}$ in Rician fading with $K_o = 2$ and $\rho = 0.8$: (a) $(M, N) = (8, 8)$ (b) $(M, N) = (8, 2)$.

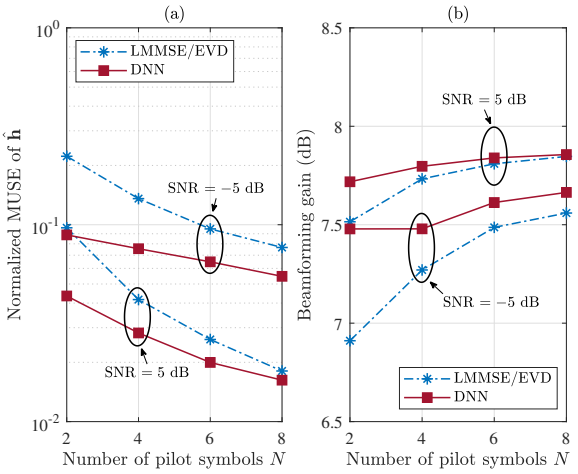

FIGURE 8. Performance of the forward channel estimators as the number N of pilot symbols varies in Rician fading when $M = 8$, $K_o = 2$, and $\rho = 0.8$: (a) normalized MUSE of $\hat{\boldsymbol{h}}$ (b) beamforming gain.

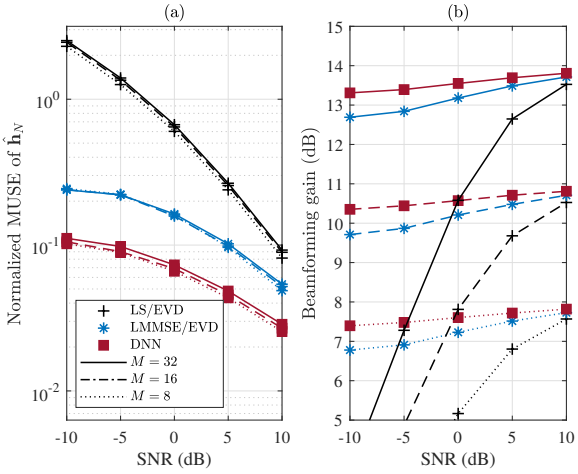

FIGURE 9. Beamforming gain as a function of the number M of antennas in Rician fading when $N = 2$, $K_o = 2$, and $\rho = 0.8$.

in Fig. 7(a) and $(M, N) = (8, 2)$ in Fig. 7(b) under Rician fading with $K_o = 2$ and $\rho = 0.8$. We provide the one-step DNN-based forward channel estimator from $\boldsymbol{Y}$ ($\tilde{\boldsymbol{Y}}$) to $\hat{h}$ in comparison with the two-step EVD-based forward channel estimators using LS, LMMSE, and mFFDNET for $\hat{\boldsymbol{G}}_N$. We also provide the mFFDNet followed by DNN for any possible performance improvement. Again, the DNN either with $\boldsymbol{Y}$ or with $\tilde{\boldsymbol{Y}}$ shows indistinguishable performance. The performance of the EVD-based forward channel estimators complies with the performance of the backscatter channel estimators shown in Fig. 5 so that mFFDNet/EVD provides the best performance among LS/EVD, LMMSE/EVD, and mFFDNET/EVD. The one-step DNN estimator provides the performance comparable to that of mFFDNet/EVD for both cases of $N = 8$ and $N = 2$. It is also observed that mFFDNet/DNN does not improve the performance further so that the DNN-based forward channel estimator is appropriate if only forward channel estimation is required for transmit beamforming.

Fig. 8 compares the performance of the forward channel estimators in Rician fading with $K_o = 2$, and $\rho = 0.8$ by varying number N of pilot symbols while fixing the number of antennas to $M = 8$. The normalized MUSE of $\hat{\boldsymbol{h}}$ is shown in Fig. 8(a) whilst the beamforming gain is provided in Fig. 8(b). The beamforming gain refers to the improvement of the received power at the BD by implementing transmit beamforming $\boldsymbol{w} = \hat{\boldsymbol{h}}^*/\|\hat{\boldsymbol{h}}\|$ for the M-antenna HAP compared with the single-antenna HAP as follows.

$$G_{BF} = \frac{\mathbb{E}[P\omega|\boldsymbol{h}^T\boldsymbol{w}|^2]}{P\omega} = \mathbb{E}\left[\frac{|\boldsymbol{h}^T\hat{\boldsymbol{h}}^*|^2}{\|\hat{\boldsymbol{h}}\|^2}\right]. \tag{37}$$

As the number of pilot symbols increases, the normalized MUSE of $\hat{\boldsymbol{h}}$ decreases and hence the beamforming gain increases. It is observed that the gain of the proposed DNN over the model-based estimator is larger in both MUSE an beamforming gain as the number of pilot symbols is smaller and the SNR gets lower since the model-based one suffers from an error propagation with reduced pilot overhead and this adverse effect is larger in the lower SNR region. In this regard, the DNN-baed forward channel estimator is more attractive than the model-based one.

We next compare the performance of the forward channel estimators as the number M of antennas increases while fixing the number of pilot symbols to $N = 2$ in Fig. 9 under Rician fading with $K_o = 2$ and $\rho = 0.8$. The normalized MUSE is similar irrespective of the number M of antennas at the HAP (that is, irrespective of the number of channel elements to be estimated) since the number of observed data also increases by using M receive antennas. The DNN provides a larger gain over the model-based ones in the normalized MUSE and beamforming gain. The results also show that the forward channel can be estimated with a small number of pilot symbols even for a large-antenna case.

This article has been accepted for publication in a future issue of this journal, but has not been fully edited. Content may change prior to final publication. Citation information: DOI 10.1109/ACCESS.2021.3134961, IEEE Access

VI. CONCLUSION

This paper has considered backscatter and forward channel estimation problems for a monostatic multiantenna BCN in a generalized fading model. We have tackled the problems with mathematical modeling and deep learning. For backscatter channel estimation, we have derived the suboptimal LMMSE estimator by analyzing the channel statistics and have presented FFDNet-based estimators toward the optimal solution. For forward channel estimation, we have proposed a DNN-based estimator with a customized loss function to replace the two-step model-based estimators. The FFDNet-based estimators for the backscatter channel were shown to outperform the LMMSE estimator as well as to improve the conventional forward channel estimator. In addition, the DNN-based forward channel estimator was shown to outperform the model-based estimators with a larger gain for less pilot overhead and more noisy channel.

.

APPENDIX A STATISTICS OF BACKSCATTER CHANNEL

We derive the mean vector $\boldsymbol{\mu}_{\mathbf{g}}$ and covariance matrix $\boldsymbol{C}_{\mathbf{g}}$ of the backscatter channel $\mathbf{g} = \text{vec}(\boldsymbol{h}\boldsymbol{h}^T)$ in terms of the mean vector $\boldsymbol{\mu}_{\boldsymbol{h}}$ and covariance matrix $\boldsymbol{C}_{\boldsymbol{h}}$.

Note that the ith element of $\mathbf{g}$ is given by

$$[\mathbf{g}]_i = h_p h_q \; i = 1, 2, \cdots, M^2, \tag{38}$$

where $p = \mod(i, M) + 1$ and $q = \lfloor i/M \rfloor + 1$. By expressing $h_p = \mu_p + \tilde{h}_p$ with $\mu_p = [\boldsymbol{\mu}_{\boldsymbol{h}}]_p$ and $\tilde{h}_p = [\tilde{\boldsymbol{h}}]_p$, we have

$$[\boldsymbol{\mu}_{\mathbf{g}}]_i = \mathbb{E}[(\mu_p + \tilde{h}_p)(\mu_q + \tilde{h}_q)] = \mu_p \mu_q \tag{39}$$

with $\mathbb{E}[\tilde{h}_p \tilde{h}_q] = 0$ from the property of the zero-mean circularly symmetric complex Gaussian $\tilde{\boldsymbol{h}}$. By examining the indices in (39), we can express $\boldsymbol{\mu}_{\mathbf{g}} = \text{vec}(\boldsymbol{\mu}_{\boldsymbol{h}} \boldsymbol{\mu}_{\boldsymbol{h}}^T)$.

The (i, j)th element of the covariance matrix $\boldsymbol{C}_{\mathbf{g}}$ is given by

$$\begin{aligned}[\boldsymbol{C}_{\mathbf{g}}]_{ij} &= \mathbb{E}[(h_p h_q - \mathbb{E}[h_p h_q])(h_m h_n - \mathbb{E}[h_m h_n])^*] \\ &= \mathbb{E}[(\mu_p \tilde{h}_q + \mu_q \tilde{h}_p + \tilde{h}_p \tilde{h}_q)(\mu_m^* \tilde{h}_n^* + \mu_n^* \tilde{h}_m^* + \tilde{h}_m^* \tilde{h}_n^*)]\end{aligned} \tag{40}$$

where $m = \mod(j, M) + 1$ and $n = \lfloor j/M \rfloor + 1$. From the properties of zero-mean circularly-symmetric complex Gaussian $\tilde{\boldsymbol{h}} \sim \mathcal{CN}(\mathbf{0}, \boldsymbol{C}_{\boldsymbol{h}})$ listed as [34]

$$\mathbb{E}[\tilde{h}_p \tilde{h}_q] = \mathbb{E}[\tilde{h}_p^* \tilde{h}_q^*] = 0, \tag{41}$$

$$\mathbb{E}[\tilde{h}_p \tilde{h}_q^* \tilde{h}_n^*] = \mathbb{E}[\tilde{h}_p^* \tilde{h}_q \tilde{h}_n] = 0, \tag{42}$$

$$\mathbb{E}[\tilde{h}_p \tilde{h}_q \tilde{h}_m^* \tilde{h}_n^*] = \mathbb{E}[\tilde{h}_p \tilde{h}_m^*]\mathbb{E}[\tilde{h}_q \tilde{h}_n^*] + \mathbb{E}[\tilde{h}_q \tilde{h}_m^*]\mathbb{E}[\tilde{h}_p \tilde{h}_n^*], \tag{43}$$

the expansion of (40) is written as

$$\begin{aligned}[\boldsymbol{C}_{\boldsymbol{b}}]_{ij} &= \mu_p \mu_m^* \mathbb{E}[\tilde{h}_q \tilde{h}_n^*] + \mu_q \mu_m^* \mathbb{E}[\tilde{h}_p \tilde{h}_n^*] + \mu_p \mu_n^* \mathbb{E}[\tilde{h}_q \tilde{h}_m^*] \\ &+ \mu_q \mu_n^* \mathbb{E}[\tilde{h}_p \tilde{h}_m^*] + \mathbb{E}[\tilde{h}_p \tilde{h}_m^*]\mathbb{E}[\tilde{h}_q \tilde{h}_n^*] + \mathbb{E}[\tilde{h}_q \tilde{h}_m^*]\mathbb{E}[\tilde{h}_p \tilde{h}_n^*].\end{aligned} \tag{44}$$

Since $\mu_p \mu_q^* = [\mathfrak{M}]_{pq}$ for $\mathfrak{M} = \boldsymbol{\mu}_{\boldsymbol{h}} \boldsymbol{\mu}_{\boldsymbol{h}}^H$ and $\mathbb{E}[\tilde{h}_p \tilde{h}_m^*] = [\boldsymbol{C}_{\boldsymbol{h}}]_{pm}$, we can express (44) as

$$\begin{aligned}[\boldsymbol{C}_{\mathbf{g}}]_{ij} &= [\mathfrak{M}]_{pm}[\boldsymbol{C}_{\boldsymbol{h}}]_{qn} + [\mathfrak{M}]_{qm}[\boldsymbol{C}_{\boldsymbol{h}}]_{pn} + [\mathfrak{M}]_{pn}[\boldsymbol{C}_{\boldsymbol{h}}]_{qm} \\ &+ [\mathfrak{M}]_{qn}[\boldsymbol{C}_{\boldsymbol{h}}]_{pm} + [\boldsymbol{C}_{\boldsymbol{h}}]_{pm}[\boldsymbol{C}_{\boldsymbol{h}}]_{qn} + [\boldsymbol{C}_{\boldsymbol{h}}]_{qm}[\boldsymbol{C}_{\boldsymbol{h}}]_{pn}.\end{aligned} \tag{45}$$

Finally, $\boldsymbol{C}_{\mathbf{g}}$ can be expressed as (14) since $[\boldsymbol{P} \otimes \boldsymbol{Q}]_{ij} = [\boldsymbol{P}]_{pm}[\boldsymbol{Q}]_{qn}$ and $[\boldsymbol{T}_{M^2}(\boldsymbol{P} \otimes \boldsymbol{Q})]_{ij} = [\boldsymbol{P}]_{qm}[\boldsymbol{Q}]_{pn}$ for $\boldsymbol{P}, \boldsymbol{Q} \in \mathbb{C}^{M \times M}$.

REFERENCES

[1] C. Xu, L. Yang, and P. Zhang, "Practical backscatter communication systems for battery-free internet of things: a tutorial and survey of recent research," *IEEE Sig. Process. Mag.*, vol. 35, no. 5, pp. 16–27, Sep. 2018.

[2] A. Bletsas *et al.*, "The art of signal processing in backscatter radio for μW (or less) internet of things: intelligent signal processing and backscatter radio enabling batteryless connectivity," *IEEE Sig. Process. Mag.*, vol. 35, no. 5, pp. 28–40, Sep. 2018.

[3] I. F. Akyildiz, A. Nak, and S. Nie, "6G and beyond: The future of wireless communications systems," *IEEE Access*, vol. 8, pp. 133995–134030, July 2020.

[4] M. Alsabah, M. A. Naser, B. M. Mahmmod, S. H. Abdulhussain, M. R. Eissa, A. Al-Baidhani, N. K. Noordin, S. M. Sait, K. A. Al-Utaibi, and F. Hashim, "6G wireless communications networks: A comprehensive survey," *IEEE Access*, vol. 9, pp. 2169–3536, Nov. 2021.

[5] S. C. Boyer and S. Roy, "Backscatter communication and RFID: coding, energy, and MIMO analysis," *IEEE Trans. Commun.*, vol. 64, no. 3, pp. 770–785, Mar. 2014.

[6] R. Correia, A. Boaventura, and N. B. Carvalho, "Quadrature amplitude backscatter modulator for passive wireless sensor in IoT applications," *IEEE Trans. Microw. Theory Techn.*, vol. 65, no. 4, pp. 1103–1110, Apr. 2017.

[7] W. Liu, K. Huang, X. Zhou, and S. Durrani, "Next generation backscatter communication: systems, techniques, and applications," *J. Wireless Com. Network*, vol. 2019, no. 69, Mar. 2019.

[8] G. Yang, C. K. Ho, and Y. L. Guan, "Multi-antenna wireless energy transfer for backscatter communication systems," *IEEE J. Sel. Areas Commun.*, vol. 33, no. 12, pp. 2974–2987, Dec. 2015.

[9] B. Clerckx, Z. B. Zawawi, and K. Huang, "Wirelessly powered backscatter communications: Waveform design and SNR-energy tradeoff." *IEEE Commun. Lett.*, vol. 21, no. 10, pp. 2234–2237, Oct. 2017.

[10] I. Krikidis, "Retrodirective large antenna energy beamforming in backscatter multi-user networks," *IEEE Wireless Commun. Lett.*, vol. 7, no. 4, pp. 678–681, Aug. 2018.

[11] Z. B. Zawawi, Y. Huang, and B. Clerckx, "Multiuser wirelessly powered backscatter communications: nonlinearity, waveform design, and SINR-energy tradeoff," *IEEE Trans. Wireless Commun.*, vol. 18, no. 1, pp. 241–253, Jan. 2019.

[12] D. Mishra and E. G. Larsson, "Optimal channel estimation for reciprocity-based backscattering with a full-duplex MIMO reader," *IEEE Trans. Sig. Process.*, vol. 67, no. 6, pp. 1662–1677, Mar. 2019.

[13] D. Mishra and E. G. Larsson, "Sum throughput maximization in multi-tag backscattering to multiantenna reader," *IEEE Trans. Commun.*, vol. 67, no. 8, pp. 5689–5705, Aug. 2019.

[14] D. Mishra and E. G. Larsson, "Multi-tag backscattering to MIMO reader: channel estimation and throughput fairness," *IEEE Trans. Wireless Commun.,* vol. 18, no. 12, pp. 5584-5599, Dec. 2019.

[15] M. Yerzhanova and Y.H. Kim, "Design of a multiuser backscatter modulation system with a multi-antenna reader," *Proc. Inter. Conf. ICT Conv. (ICTC)*, pp. 988–990, Jeju, Korea, Oct. 2020.

[16] Y. Ye, L. Shi, X. Chu and G. Lu, "Throughput fairness guarantee in wireless powered backscatter communications with HTT," *IEEE Wireless Commun. Lett.,* vol. 10, no. 3, pp. 449–453, Mar. 2021.

[17] G. Sacarelo and Y.H. Kim, "Beamforming and reflection coefficient control for multiantenna backscatter communication With nonorthogonal multiple access," *IEEE Access,* vol. 9, pp. 56104–56114, Apr. 2021.

[18] K. Han and K. Huang, "Wirelessly powered backscatter communication networks: modeling, coverage, and capacity," *IEEE Trans. Wireless Commun.*, vol. 16, no. 4, pp. 2548–2561, Apr. 2017.

[19] N. Van Huynh, D. T. Hoang, X. Lu, D. Niyato, P. Wang, and D. I. Kim, "Ambient backscatter communications: A contemporary survey," *IEEE Commun. Surveys & Tutor.*, vol. 20, no. 4, pp. 2889–2922, 4Q 2018.

[20] G. Yang, D. Yuan, Y.-C. Liang, R. Zhang, and V. C. M. Leung, "Optimal resource allocation in full-duplex ambient backscatter communication networks for wireless-powered IoT," *IEEE Internet Things J.*, vol. 6, no. 2, pp. 2612–2625, Apr. 2019.

[21] Q. Zhang, L. Zhang, Y.-C. Liang, and P.-Y. Kam, "Backscatter-NOMA: A symbiotic system of cellular and Internet-of-Things networks," *IEEE Access,* vol. 7, pp. 20000–20013, 2019.

[22] C. Yang , X. Wang , and K.-W. Chin, "On max–min throughput in backscatter-assisted wirelessly powered IoT," *IEEE Internet of Things J.*, vol. 7, no. 1, pp. 137–147, Jan. 2020.
[23] H. Huang, J. Yang, H. Huang, Y. Song, and G. Gui, "Deep learning for super-resolution channel estimation and DOA estimation based massive MIMO system," *IEEE Trans. Veh. Technol.*, vol. 67, no. 9, pp. 8549–8560, Sep. 2018.
[24] J. M. Kang, C. J. Chun, I. M. Kim, "Deep-learning-based channel estimation for wireless energy transfer," *IEEE Commun. Lett.*, vol. 22, no. 11, pp. 2310–2313, Nov. 2018.
[25] C. J. Chun, J. M. Kang, and I. M. Kim, "Deep learning-based channel estimation for massive MIMO systems," *IEEE Wireless Commun. Lett.*, vol. 8, no. 4, pp. 1228–1231, Aug. 2019.
[26] Y. Jin, J. Zhang, S. Jin, and B. Ai, "Channel estimation for cell-free mmWave massive MIMO through deep learning," *IEEE Trans. Veh. Technol.*, vol. 68, no. 10, pp. 10325–10329, Oct. 2019.
[27] Z. Gao, Y. Wang, X. Liu, F. Zhou, and K. Wong, "FFDNet-based channel estimation for massive MIMO visible light communication systems," *IEEE Wireless Commun. Lett.*, vol. 9, no. 3, pp. 340–343, Mar. 2020.
[28] S. Liu, Z. Gao, J. Zhang, M. D. Renzo, and M. S. Alouini, "Deep denoising neural network assisted compressive channel estimation for mmWave intelligent reflecting surfaces," *IEEE Trans. Veh. Technol.*, vol. 69, no. 8, pp. 9223–9228, Aug. 2020.
[29] X. Liu, Y. Li, B. Vucetic, and D. W. K. Ng, "Deep residual learning-assisted channel estimation in ambient backscatter communication," *IEEE Wireless Commun. Lett.*, vol. 10, no. 2, pp. 339–343, Feb. 2021.
[30] N. K. Kundu and M. R. McKay, "Channel estimation for reconfigurable intelligent surface aided MISO communications: from LMMSE to deep learning solutions," *IEEE Open J. Commun. Society*, vol. 2, pp. 471–487, Mar. 2021.
[31] K. Zhang, W. Zuo, Y. Chen, D. Meng and L. Zhang, "Beyond a Gaussian Denoiser: Residual Learning of Deep CNN for Image Denoising," in IEEE Transactions on Image Processing, vol. 26, no. 7, pp. 3142-3155, July 2017
[32] K. Zhang, W. Zuo, and L. Zhang, "FFDNet: Toward a fast and flexible solution for CNN-based image denoising," *IEEE Trans. Imag Process.*, vol. 27, no. 9, pp. 4608–4622, Sept. 2018.
[33] O. Ozdogan, E. Bjornson, and E. G. Larsson, "Massive MIMO with spatially correlated Rician fading channels," *IEEE Trans. Commun.*, vol. 67, no. 5, pp. 3234–3250, May. 2019.
[34] S. M. Kay, *Fundamentals of Statistical Signal Processing: Estimation Theory*, Englewood Cliffs, NJ, Prentice Hall, 1993.
[35] K. He and J. Sun, "Convolutional neural networks at constrained time cost," *Proc. IEEE Conf. Comput. Vis. Pattern Recognit. (CVPR)* , pp.5553–5660, Jun. 2015.

MOLDIR YERZHANOVA received the B.S. degree in electrical and electronic engineering from Nazarbayev University, Kazakhstan, in 2018. She is currently pursuing the M.S. degree in electronic and information convergence engineering in Kyung Hee University, Yongin, Korea. Her current research interests include wireless communications and deep learning techniques for estimation and optimization.

YUN HEE KIM (S'97-M'00-SM'05) received the B.S.E. (*summa cum laude*), M.S.E., and Ph.D. degrees in electrical engineering from Korea Advanced Institute of Science and Technology, Daejeon, Korea, in 1995, 1997, and 2000, respectively. From Sept. 2000 to Aug. 2004, she was with Electronics and Telecommunications Research Institute, Daejeon, Korea, as a Senior Member of Research Staff. In Sept. 2004, she joined the Department of Electronic Engineering, Kyung Hee University, Yongin, Korea, where she is currently a Professor. In 2000 and 2011, she was with the Department of Electrical and Computer Engineering, University of California at San Diego, La Jolla, CA, USA, as a Visiting Researcher. Her research interests include wireless/mobile communications, statistical signal processing, and artificial intelligence for wireless networks.